NUCLEAR SCIENCE AND ENGINEERING: **178**, 66–75 (2014)

Measurement of the $^{238}U(n,\gamma)^{239}U$ and $^{238}U(n,2n)^{237}U$ Reaction Cross Sections Using a Neutron Activation Technique at Neutron Energies of 8.04 and 11.90 MeV

R. Crasta and S. Ganesh

Mangalore University, Department of Studies in Physics, Microtron Centre
Mangalagangotri-574 199, India

and

H. Naik* and A. Goswami

Bhabha Atomic Research Centre, Radiochemistry Division
Mumbai-400085, India

S. V. Suryanarayana, S. C. Sharma, and P. V. Bhagwat

Bhabha Atomic Research Centre, Nuclear Physics Division
Mumbai-400085, India

B. S. Shivashankar

Manipal University, Department of Statistics
Manipal-576 104, Karnataka, India

V. K. Mulik

University of Pune, Department of Physics
Pune-411 007, India

and

P. M. Prajapati

The M. S. University of Baroda, Physics Department
Vadodara-390002, India

Received October 27, 2011
Accepted February 11, 2013
http://dx.doi.org/10.13182/NSE11-90

*E-mail: naikhbarc@yahoo.com

Abstract—*The (n,γ) and (n,2n) capture cross sections of ^{238}U have been measured at neutron energies of 8.04 ± 0.30 and 11.90 ± 0.35 MeV from the $^{7}Li(p,n)$ reaction using an activation and off-line gamma-ray spectrometric technique. The experimentally determined $^{238}U(n,\gamma)$ and $^{238}U(n,2n)$ reaction cross sections were compared with the evaluated data of ENDF/B-VII.0, JENDL-4.0, JEFF-3.1/A, and CENDL-3.1. The experimental values were found to be in agreement with the evaluated value based on ENDF/B-VII.0, JENDL-4.0, and JEFF-3.1/A but not with CENDL-3.1. The present measurement has been compared with literature data in a wide range of neutron energies. The $^{238}U(n,\gamma)^{239}U$ and $^{238}U(n,2n)^{237}U$ reaction cross sections were also calculated theoretically using the TALYS 1.4 computer code and compared with the experimental data.*

I. INTRODUCTION

The measurement of neutron activation cross sections and its improved nuclear database play a vital role in the design and safe operation of various nuclear systems such as Generation IV nuclear reactors, fusion reactors, and accelerator-driven subcritical systems[1,2] (ADSs). The heavy water reactor concept allows the use of natural uranium as a fuel without the need for its enrichment. Light water reactors use ^{235}U as a fuel enriched to ~3%. Breeder nuclear reactors are based on the ^{238}U-^{239}Pu fuel cycle, in which transmutation of the fertile isotope ^{238}U to the fissile isotope ^{239}Pu takes place. Fast breeder reactors (FBRs) are designed with a core containing ~15% fissile plutonium and 85% ^{238}U (depleted uranium) in the form of mixed oxides or carbides surrounded by a blanket of depleted uranium. The ^{239}Pu used in fast reactors is first generated in a research reactor from the $^{238}U(n,\gamma)^{239}U$ reaction followed by two successive beta decays.

Thus, the neutron capture cross section of ^{238}U is an important parameter for the design of any nuclear system based on the ^{238}U-^{239}Pu fuel cycle and in particular for fast reactor[3–6] calculations. This is because in fast reactors, the production of fissile nucleus ^{239}Pu depends on the $^{238}U(n,\gamma)$ reaction cross section, which is required with an accuracy of 1% to 2% for predicting the dynamical behavior of complex arrangements[7,8] and safety.

In FBRs the most important region for neutron capture of ^{238}U lies between 10 and 100 keV (Ref. 9). However, the neutron energy in fast reactors is on the higher side, i.e., from 10 keV to 15 MeV. At the higher neutron energy the $^{238}U(n,2n)^{237}U$ reaction starts besides the (n,γ) reaction. Thus, the $^{238}U(n,\gamma)$ and $^{238}U(n,2n)$ reaction cross sections at higher neutron energy have a strong impact on fast reactor performance and safety assessment.[10] In addition, nuclear data of ^{238}U such as (n,f), (n,γ), and (n,xn) cross sections are also important for fusion reactor and ADS calculations.

There are some measurements of the $^{238}U(n,\gamma)$ reaction cross section from thermal to 20 MeV based on physical measurements[11–17] and an activation technique.[18–26] However, sufficient data on the $^{238}U(n,2n)$ reaction cross section are available at different neutron energies from gamma-ray spectrometry and neutron activation methods.[26–31] Different evaluations such as ENDF/B-VII.0 (Ref. 32), JENDL 4.0 (Ref. 33), JEFF-3.1/A (Ref. 34), and CENDL-3.1 (Ref. 35) are also available for the $^{238}U(n,\gamma)$ and $^{238}U(n,2n)$ reaction cross sections.

Ding and Guo[36] reviewed the $^{238}U(n,\gamma)$ reaction cross section within neutron energies of 1 keV to 20 MeV. From the experimental data,[11–31] it was observed that the $^{238}U(n,\gamma)$ reaction has numerous resonance cross sections from thermal energy to 0.1 MeV. For neutron energies above 0.1 to 20 MeV, Naik et al.[26] compared experimental data[11–31] with different evaluated data.[32–36] They found that the CENDL-3.1 evaluated data[35] are comparable to most of the experimental $^{238}U(n,\gamma)$ reaction cross-section data above 0.1 to 20 MeV. However, the CENDL-3.1 trend[35] is entirely different from that of other evaluations.[32–34] The experimental data of McDaniels et al.[16] within neutron energies of 7 to 14 MeV and Naik et al.[26] at 3.7 and 9.85 MeV as well as the data of Leipunskiy et al.[18] and Panitkin and Tolstikov[19] below 4 MeV only follow the trends of the ENDF/B-VII.0 (Ref. 32), JENDL 4.0 (Ref. 33), and JEFF-3.1/A (Ref. 34) evaluations. However, the $^{238}U(n,\gamma)$ reaction cross-section data of Leipunskiy et al.[18] and Panitkin and Tolstikov[20] as well as the data of Ding and Guo[36] within neutron energies of 4 to 9 MeV and 14 to 20 MeV are higher than the evaluated value of ENDF/B-VII.0 (Ref. 32), JENDL 4.0 (Ref. 33), and JEFF-3.1/A (Ref. 34). Thus, it is very important to measure the $^{238}U(n,\gamma)$ and $^{238}U(n,2n)$ reaction cross sections within neutron energies of 4 to 20 MeV to test different evaluations[32–35] in addition to their applications in reactor technology.

To examine the above aspects, in this work we use an activation technique followed by off-line gamma-ray spectrometry[26] to measure the $^{238}U(n,\gamma)$ and $^{238}U(n,2n)$ reaction cross sections at neutron energies of 8.04 ± 0.30 and 11.90 ± 0.35 MeV from the $^{7}Li(p,n)$ reaction. The experimentally obtained reaction cross sections were compared with the evaluated nuclear data of ENDF/B-VII.0 (Ref. 32), JENDL 4.0 (Ref. 33), JEFF-3.1/A (Ref. 34), and CENDL-3.1 (Ref. 35). The $^{238}U(n,\gamma)$ and $^{238}U(n,2n)$ reaction cross sections were also calculated using the TALYS 1.4 code[37] and compared with the experimental data.

II. DESCRIPTION OF THE EXPERIMENT

Average neutron energies of 8.04 ± 0.30 and 11.90 ± 0.35 MeV were produced by the $^{7}Li(p,n)$

reaction, using the 14UD Bhabha Atomic Research Centre (BARC)–Tata Institute of Fundamental Research (TIFR) Pelletron facility at Mumbai, India, as done earlier by Naik et al.[26] The lithium foil was made up of natural lithium with 3.7 mg/cm^2 thickness and is sandwiched between two tantalum foils of different thicknesses. The thinner tantalum foil faced the proton beam with 4 mg/cm^2 thickness, in which the degradation of the proton energy is only 30 keV. The thicker tantalum foil of 0.025 mm, which is located behind the lithium foil, is sufficient to stop the proton beam. The natural uranium metal foil wrapped with 0.025-mm-thick super-pure aluminum foil was mounted at 0 deg with respect to the beam direction at a distance of 2.0 cm behind the Ta-Li-Ta stack. The experimental arrangement is shown in Fig. 1.

Separate sets of samples were made for irradiation for two different neutron energies. In the first set the thickness of uranium foil is 395.1 mg/cm^2, whereas in the second set it is 344.1 mg/cm^2. The samples were irradiated for 5 to 7 h depending upon the proton beam energy facing the tantalum target. The proton beam energies were 10 and 14 MeV, and the proton current during the irradiation was 270 nA at 10 MeV and 300 nA at 14 MeV, respectively. The corresponding average neutron energies impinging on the U targets were 8.04 ± 0.30 MeV and 11.90 ± 0.35 MeV, respectively. The irradiated samples were cooled for 3 to 4 h, mounted on Perspex plates, and taken for gamma-ray spectrometry. The activities of the radionuclides produced from irradiated U samples were measured using an energy- and efficiency-calibrated 80-cm^3 high-purity germanium detector coupled to a personal computer–based 4K channel analyzer.

A typical gamma-ray spectrum of irradiated ^{238}U is shown in Fig. 2. The measurements were repeated several times to follow the decay of the radionuclides. Measurements were done at a suitable distance from the detector to keep the dead time within 5%. The detection efficiency as a function of gamma-ray energy was determined by using the standard sources of ^{133}Ba and ^{152}Eu. The standard sources of ^{133}Ba and ^{152}Eu were chosen

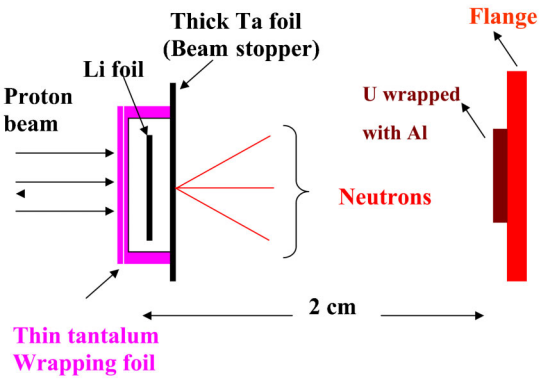

Fig. 1. Schematic diagram showing the arrangement used for neutron irradiation.

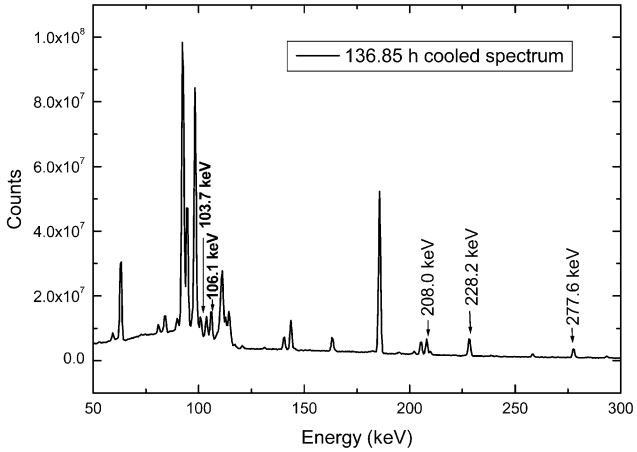

Fig. 2. Gamma-ray spectrum of irradiated ^{238}U showing the gamma-ray energy of ^{237}U and ^{239}Np.

to cover the energy range from 53.16 to 1408.01 keV to avoid so many sources having single or few gamma lines. The gamma-ray counting of the standard sources was done at the same geometry keeping in mind the summation error. This was checked by comparing the efficiency obtained from gamma-ray counting of standards such as ^{241}Am [59.54 (35.9%) keV], ^{137}Cs [661.66 (85.1%) keV], ^{54}Mn [834.55 (99.976%) keV], and ^{60}Co [1173.24 (99.994%) and 1332.5 (99.986%) keV]. The detector efficiency was 20% at 1332.5 keV relative to a 3-in.-diam × 3-in.-length NaI(Tl) detector. The uncertainty in the efficiency was 2% to 3%. The resolution of the detector system had a full-width at half-maximum of 1.8 keV at 1332.5 keV of ^{60}Co.

III. ANALYSIS OF THE EXPERIMENT AND RESULTS

III.A. Calculation of the Neutron Energy

Natural lithium consists of ^{6}Li and ^{7}Li isotopes with abundances 7.42% and 92.58%, respectively. Neutrons are generated by the ^{7}Li(p,n) reaction. The Q-value for the ^{7}Li(p,n)^{7}Be reaction to the ground state is −1.644 MeV, whereas for the first excited state it is 0.431 MeV above the ground state leading to an average Q-value of −2.079 MeV. The threshold for the ground state of ^{7}Be is 1.881 MeV, whereas for the first excited state it is 2.38 MeV. For the ^{7}Li(p,n) reaction, a second group of neutrons at $E_P \geq 2.4$ MeV is also produced due to the population of the first excited state of ^{7}Be. The proton energies for the present experiment are 10 and 14 MeV. The degradation of the proton energy on the front thin tantalum foil of 4 mg/cm^2 thickness is only 30 keV. Thus, for proton energies of 10 and 14 MeV, the corresponding first groups of n_0 neutron energies are 8.12 and 12.12 MeV to the ground state of ^{7}Be. For the first excited state of ^{7}Be, the neutron energies of the second group of neutrons n_1

will be 7.62 and 11.62 MeV, respectively. When the proton energy exceeds 4.5 MeV, fragmentation of ^{8}Be to ^{4}He + ^{3}He + n (Q = −3.23 MeV) occurs, and other reaction channels also open to give continuous neutron distribution besides n_0 and n_1 groups of neutrons.

The branching ratios for the ground and first excited states of ^{7}Be up to a proton energy of 7 MeV are given in Refs. 38 and 39, whereas for proton energies from 4.2 to 26 MeV, they are given in Ref. 40. Besides the n_0 and n_1 groups, continuous neutron spectra for the proton energies of 10 and 14 MeV have been generated using the neutron energy distribution from Refs. 40 and 41.

The neutron energy spectrum obtained from the ^{7}Li(p,n) reaction for proton energies of 10 and 14 MeV are given in Figs. 3 and 4, respectively. It can be seen from Fig. 3 that for a proton energy of 10 MeV, the neutrons from the n_0 and n_1 groups have the peak at 8.12 and 7.62 MeV, respectively. Based on Ref. 40 for a proton energy of 10 MeV, the contributions to the n_0 and n_1 groups of neutrons are 50.61% and 49.39%, respectively. Thus, a proton energy of 10 MeV leads to an average neutron energy of $8.12 \times 0.5061 + 7.62 \times 0.4939 =$ 7.873 MeV. From Fig. 3, the flux weighted average neutron energy above 6 MeV gives a value of 8.04 ± 0.30 MeV, which is closer to the value of 7.873 MeV.

Thus, we have used the neutron energy 8.04 ± 0.30 MeV for the proton energy of 10 MeV. A cutoff energy of 6 MeV is considered because of neutron tail distribution as well as the minimum flux at this energy from a different excited state. In the case of a proton energy of 14 MeV, the neutron spectrum was obtained from Ref. 41. For this proton energy, the contributions to the n_0 and n_1 groups of neutrons are not available in Ref. 41, and they are not resolved in the experimental spectrum (Fig. 4). Thus, flux weighted average neutron energy above 10.5 MeV gives the value of 11.90 ± 0.35 MeV. The cutoff energy of 10.5 MeV was chosen based on the same argument given above.

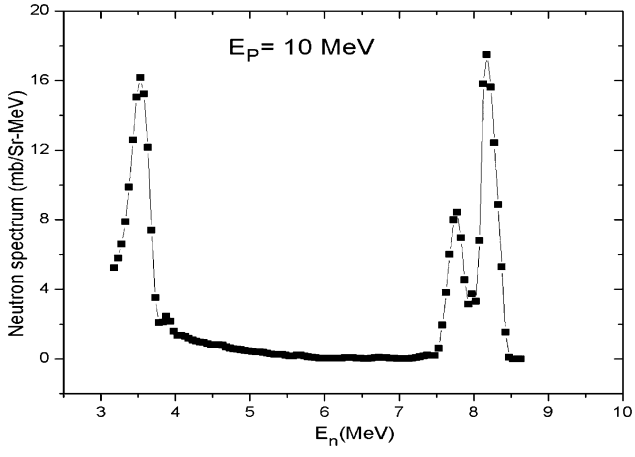

Fig. 3. Neutron spectrum for ^{7}Li(p,n)^{7}Be reaction at E_P = 10 MeV calculated using the results of Poppe et al.[40]

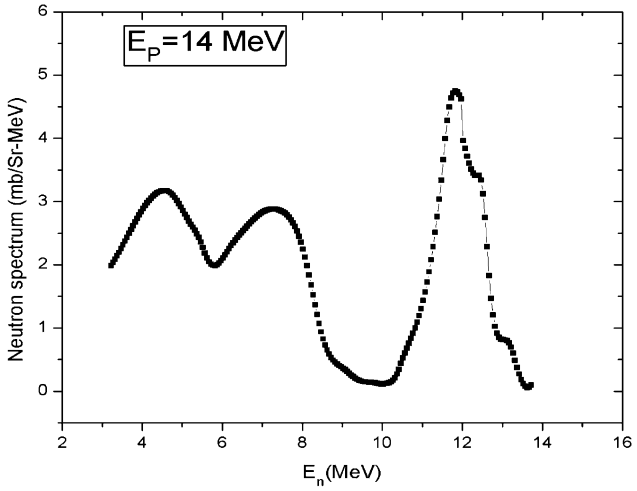

Fig. 4. Interpolated neutron spectrum in ^{7}Li(p,n) reaction at E_P = 14 MeV obtained from the neutron spectrum at E_P =15 MeV of Mashnik et al.[41]

III.B. Calculation of the Neutron Flux

The neutron flux is usually obtained by using ^{197}Au(n,γ)^{198}Au and ^{115}In(n,n')^{115m}In reaction cross sections for monoenergetic nuclear reactions. For thermal neutrons the photopeak activity of the 411.8-keV gamma-line for ^{198}Au from the ^{197}Au(n,γ) reaction is used to find the neutron flux. For higher-energy neutrons, the photopeak activity of the 336.2-keV gamma-line of the ^{115m}In from the ^{115}In(n,n') reaction is used for flux determination. In the present work the neutron beam was produced from the ^{7}Li(p,n) reaction, where the neutron energy is on the higher side and not exactly monoenergetic. This is due to the contribution from the second group as well as a tailing resulting from the breakup ^{8}Be → ^{4}He + ^{3}He + n, which has a significant contribution.

It can be seen from Refs. 40 and 41 that the tailing region of the low-energy neutrons is quite significant. Within this range of neutron energy, the ^{115}In(n,n')^{115m}In reaction cross section changes continuously.[42] For this purpose, the neutron flux was calculated using the yield Y of fission products as ^{135}I and ^{97}Zr from Refs. 43 and 44. The neutron flux and the observed photopeak activities A_{obs} for gamma-lines of the respective nuclide are related by Eq (1):

$$\varphi = \frac{A_{obs}(CL/CT)\lambda}{N\sigma_f Ya\varepsilon(1-e^{-\lambda t})(e^{-\lambda T})(1-e^{-\lambda CL})}\ , \qquad (1)$$

where

N = number of target atoms

Y = yield of the fission product taken from Refs. 43 and 44

σ_f = fission cross section, which is given in Refs. 32 through 35 and 45. The ^{238}U(n,f)

cross sections from Refs. 32 through 35 and 45 are comparable. In view of this, in the present work, the $^{238}U(n,f)$ cross section from Ref. 32 has been used.

a = branching intensity

ε = detection efficiency for gamma-lines of the nuclide of interest

γ = decay constant for the isotope

t, T = irradiation and cooling times, respectively

CL, LT = clock time and live time of counting, respectively.

In Eq. (1), the *CL/LT* term has been used for dead-time correction. The gamma-ray energies and the nuclear spectroscopic data such as the half-lives and branching ratios of the reaction products are taken from Refs. 46, 47, and 48 and are given in Table I. The observed photopeak activities A_{obs} of the respective radionuclide were obtained using the PHAST peak fitting program.[49]

The neutron fluxes for neutron energies of 8.04 ± 0.30 and 11.90 ± 0.35 MeV corresponding to proton energies of 10 and 14 MeV were calculated using Eq. (1) and were found to be $(3.84 \pm 0.06) \times 10^6$ and $(1.30 \pm 0.02) \times 10^7$ n/cm^2·s, respectively. On the other hand, the neutron fluxes for the $^{238}U(n,2n)$ reaction at average neutron energies of 8.04 ± 0.30 and 11.90 ± 0.35 MeV were obtained as $(1.83 \pm 0.03) \times 10^6$ and $(8.02 \pm 0.14) \times 10^6$ n/cm^2·s, respectively. These values were obtained based on the ratio of the neutron flux of the neutron spectrum of Refs. 40 and 41 for the $(n,2n)$ reaction above its threshold to the total flux.

III.C. Determination of $^{238}U(n,\gamma)^{239}U$ and $^{238}U(n,2n)^{237}U$ Reaction Cross Sections and Their Results

The neutron irradiation of ^{238}U resulted in production of ^{239}U and ^{237}U through (n,γ) and $(n,2n)$ reactions, respectively. The decay data of the radioactive products for the (n,γ) and $(n,2n)$ reactions are taken from Refs. 46 and 47, which are presented in Table I. The radionuclide ^{239}U ($t_{1/2}$ = 23.45 m), which is produced from the $^{238}U(n,\gamma)^{239}U$ reaction, gives rise to ^{239}Np ($t_{1/2}$ = 2.357 days) by the β^- decay process. Thus, after 6 h from the end of irradiation, ^{239}U decays almost completely to ^{239}Np. In view of this, the $^{238}U(n,\gamma)$ reaction cross section was calculated from the observed photopeak activity of ^{239}Np from the gamma-ray spectrum of the long cooled sample. The ^{239}Np radionuclide was identified through the characteristic gamma-lines of 103.73, 106.13, 228.4, and 277.85 keV. However, the $^{238}U(n,\gamma)$ reaction cross section was calculated from the photopeak activities of the 103.73- and 277.85-keV gamma-lines of ^{239}Np. The photopeak activities of the 106.13- and 228.2-keV gamma-lines of ^{239}Np from the gamma-ray spectrum were not used. The $^{238}U(n,2n)$ reaction cross section was calculated from the observed photopeak activity of the 208.0-keV gamma-line of ^{237}U from the gamma-ray spectrum of a sufficiently cooled sample. The photopeak activity of the 101.1-keV gamma-line of ^{237}U from the gamma-ray spectrum was not used.

For the calculation of the $^{238}U(n,\gamma)$ and $^{238}U(n,2n)$ reaction cross section σ, Eq. (2) was used:

$$\sigma = \frac{A_{obs}\left(\frac{CL}{LT}\right)\lambda}{N\varphi a\varepsilon(1-e^{-\lambda t})(e^{-\lambda T})(1-e^{-\lambda CL})}\ , \qquad (2)$$

where all terms in Eq. (2) have similar meanings as in Eq. (1). The experimentally determined $^{238}U(n,\gamma)$ reaction cross sections at average neutron energies of 8.04 ± 0.30 and 11.90 ± 0.35 MeV are 5.93 ± 0.08 and 3.50 ± 0.18 mb, respectively. Similarly, the experimentally determined $^{238}U(n,2n)$ reaction cross section at average neutron energies of 8.04 ± 0.30 and 11.90 ± 0.35 MeV are 1044.1 ± 30.78 and 1231.39 ± 58.95 mb, respectively. These $^{238}U(n,\gamma)$ cross-section values are much higher than the expected values because of the contribution from the low-energy neutron reaction cross section.

TABLE I

Nuclear Spectroscopic Data Used in the Calculation

Nuclide	Half-Life	Gamma-Ray Energy (keV)	Gamma-Ray Abundance (%)	Reference
^{115m}In	4.486 h	336.2	45.9	46
^{237}U	6.75 days	101.1	26.0	48
		208.0	21.2	48
^{239}U	23.45 min	74.7	52.2	47
^{239}Np	2.357 days	103.7	23.9	47
		106.1	22.7	47
		228.2	10.8	47
		277.6	14.4	47

The contributions of the $^{238}U(n,\gamma)$ reaction cross section arising from the tail region of the neutron spectrum have been estimated by folding the evaluated ENDF/B-VII.0 (Ref. 32) and JENDL-4.0 (Ref. 33) cross sections with the neutron flux distributions of Refs. 40 and 41. At a proton energy of 10 MeV, the contributions to the total $^{238}U(n,\gamma)$ reaction cross section were evaluated to be 4.86 and 3.88 mb from ENDF/B-VII.0 (Ref. 32) and JENDL-4.0 (Ref. 33), respectively. Similarly, at a proton energy of 14 MeV, the contributions to the $^{238}U(n,\gamma)$ reaction cross section from the above evaluations are 2.38 and 1.81 mb from ENDF/B-VII.0 (Ref. 32) and JENDL-4.0 (Ref. 33), respectively.

It can be seen from above evaluations that the correction to the $^{238}U(n,\gamma)$ reaction cross section due to the tail part of the neutron spectrum is systematically lower based on JENDL-4.0 compared to ENDF/B-VII.0. Thus, we have used the $^{238}U(n,\gamma)$ reaction cross-section correction based on the ENDF/B-VII.0 evaluation only. Further reason for this is given in Sec. IV.

The experimental $^{238}U(n,\gamma)$ reaction cross sections of 1.07 ± 0.08 and 1.12 ± 0.18 mb at average neutron energies of 8.04 ± 0.30 and 11.90 ± 0.35 MeV corresponding to proton energies of 10 and 14 MeV were obtained after removing the tailing contribution based on ENDF/B-VII.0. However, there is a big difference in the $^{238}U(n,\gamma)$ reaction cross section due to the tail part of the neutron spectrum based on ENDF/B-VII.0 (Ref. 32) and JENDL-4.0 (Ref. 33).

Thus, after taking care of the error from both evaluations, the actual experimental $^{238}U(n,\gamma)$ reaction cross sections of 1.07 ± 0.23 and 1.12 ± 0.32 mb at average neutron energies of 8.04 ± 0.30 and 11.90 ± 0.35 MeV, respectively, the error in the $^{238}U(n,\gamma)$ reaction cross-section value is based on replicate measurements besides the error from the tailing part correction based on the ENDF/B-VII.0 (Ref. 32) and JENDL-4.0 (Ref. 33) evaluations. The $^{238}U(n,2n)$ reaction cross section at average neutron energies of 8.04 ± 0.30 and 11.90 ± 0.35 MeV corresponding to proton energies of 10 and 14 MeV were obtained as 1044.1 ± 30.78 and 1231.39 ± 58.95 mb, respectively.

The uncertainties for the $^{238}U(n,\gamma)$ and $^{238}U(n,2n)$ reaction cross sections are based on replicate measurements. Thus, overall uncertainty is the quadratic sum of both statistical and systematic errors. The random error in the observed activity is primarily due to counting statistics, which is estimated to be 5% to 10%. The counting statistics error of 5% is for the photopeak activities of 103.73- and 277.83-keV gamma rays of ^{239}Np. On the other hand, an error of 10% is for the photopeak activity of the 208.0-keV gamma rays of ^{237}U. This can be determined by accumulating the data for an optimum time period that depends on the half-life of the nuclides of interest. The systematic errors are due to uncertainties in neutron flux estimation ($\sim$4%), the irradiation time ($\sim$2%), the detection efficiency calibration ($\sim$3%), the half-life of the fission products, and the gamma-ray abundances ($\sim$2%). Thus, the total systematic error is $\sim$6%. The overall uncertainty is found to range between 7.5% and 11.5%, coming from the combination of a statistical error of 5% to 10% and a systematic error of 6%. Thus, after incorporating an error of 7.5%, the final $^{238}U(n,\gamma)$ reaction cross sections at average neutron energies of 8.04 ± 0.30 and 11.90 ± 0.35 MeV are 1.07 ± 0.24 and 1.12 ± 0.33 mb, which are given in Table II. Similarly, after incorporating an error of 11.5%, the final $^{238}U(n,2n)$ reaction cross sections

TABLE II

The $^{238}U(n,\gamma)$ and $^{238}U(n,2n)$ Reaction Cross Sections at Different Neutron Energies

Neutron Energy (MeV)	Neutron Flux (n/cm^2·s)	Cross Section (mb)				
		Experimental	ENDF/B-VII.0	JENDL-4.0	JEFF-3.1/A	CENDL-3.1
$^{238}U(n,\gamma)$						
8.04 ± 0.3	$(3.84 \pm 0.06) \times 10^6$	1.07 ± 0.24	1.06 to 1.02[a]	0.82 to 1.08[a]	1.14 to 1.05[b]	2.20 to 1.50[a]
11.9 ± 0.35	$(1.30 \pm 0.02) \times 10^7$	1.12 ± 0.33	1.24 to 1.05[c]	0.91 to 0.79[c]	1.23 to 1.02[d]	0.87 to 0.97[c]
$^{238}U(n,2n)$						
8.04 ± 0.3	$(1.83 \pm 0.03) \times 10^6$	1044.05 ± 123.95	928.48 to 1212.9[a]	784.54 to 1204.77[a]	826.61 to 1228.05[a]	412.64 to 1298.4[b]
11.9 ± 0.35	$(8.02 \pm 0.01) \times 10^6$	1231.39 ± 153.41	1441.08 to 1361.00[c]	1445.32 to 1405.6[c]	1477.44 to 1386.32[c]	1390.9 to 1166.7[d]

[a]The neutron energy ranges for $^{238}U(n,\gamma)$ and $^{238}U(n,2n)$ reactions are 7.5 to 8.5 MeV.
[b]The neutron energy ranges for $^{238}U(n,\gamma)$ and $^{238}U(n,2n)$ reactions are 7 to 9 MeV.
[c]The neutron energy ranges for $^{238}U(n,\gamma)$ and $^{238}U(n,2n)$ reactions are 11.5 to 12.5 MeV.
[d]The neutron energy ranges for $^{238}U(n,\gamma)$ and $^{238}U(n,2n)$ reactions are 11.0 to 13.0 MeV.

at average neutron energies of 8.04 ± 0.30 and 11.90 ± 0.35 MeV are 1044.1 ± 123.95 and 1231.39 ± 153.41 mb, which are given in Table II. The evaluated ^{238}U(n,γ) and ^{238}U(n,2n) reaction cross sections from ENDF/B-VII.0 (Ref. 32), JENDL-4.0 (Ref. 33), JEFF-3.1/A (Ref. 34), and CENDL-3.1 (Ref. 35) are also given in Table II for comparison.

IV. DISCUSSION

The ^{238}U(n,γ) and the ^{238}U(n,2n) reaction cross sections at average neutron energies E_n of 8.04 ± 0.30 and 11.90 ± 0.35 MeV shown in Table II are determined using an activation and off-line gamma-ray spectrometric technique. The (n,γ) and (n,2n) capture cross sections of ^{238}U have been measured at neutron energies of 8.04 ± 0.30 and 11.90 ± 0.35 MeV from the ^{7}Li(p,n) reaction using the activation and off-line gamma-ray spectrometric technique. The technique used in the present work for determining the ^{238}U(n,γ) and the ^{238}U(n,2n) reaction cross sections at higher-energy neutrons is similar to the approach used by Naik et al.[26] but is different from the conventional methods with monoenergetic neutrons.[13–31] The experimentally measured ^{238}U(n,γ) and ^{238}U(n,2n) reaction cross sections were compared with the literature data,[16,27] based on monoenergetic neutrons, which is shown in Figs. 5 and 6. They were found to be in good agreement, which shows the validity of the present approach. In Table II, the experimentally determined ^{238}U(n,γ) and ^{238}U(n,2n) reaction cross sections from the present work are compared with evaluated nuclear data from ENDF/B-VII.0 (Ref. 32), JENDL-4.0 (Ref. 33), JEFF-3.1/A (Ref. 34), and CENDL-3.1 (Ref. 35).

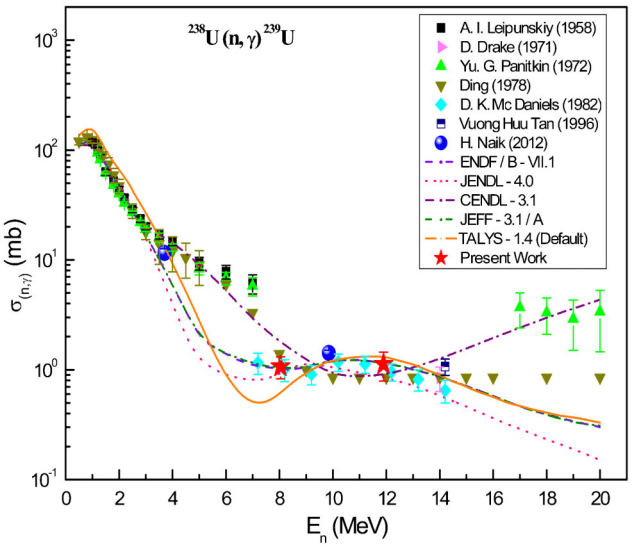

Fig. 5. Plot of experimental and evaluated ^{238}U(n,γ) reaction cross sections as a function of neutron energy.

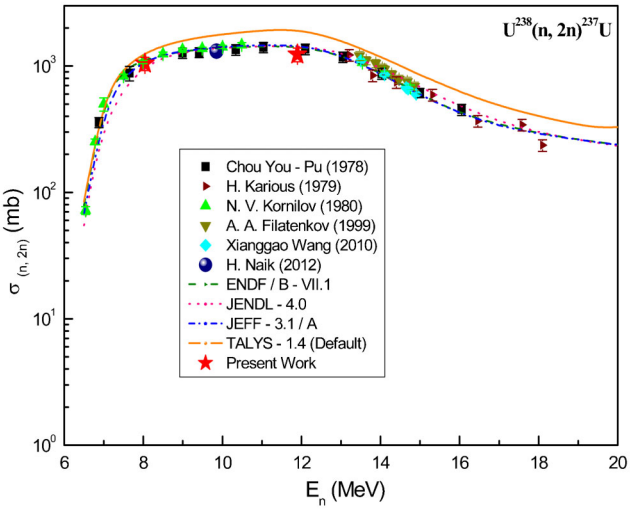

Fig. 6. Plot of experimental and evaluated ^{238}U(n,2n) reaction cross sections as a function of neutron energy.

It can be seen from Table II that the ^{238}U(n,γ) and ^{238}U(n,2n) reaction cross sections at average neutron energies of 8.04 ± 0.30 and 11.90 ± 0.35 MeV are within the range of the evaluated data of ENDF/B-VII.0 (Ref. 32), JENDL 4.0 (Ref. 33), and JEFF-3.1/A (Ref. 34). However, the evaluated ^{238}U(n,γ) reaction cross section from CENDL-3.1 (Ref. 35) shown in Table II is not in good agreement with the present experimental value. In order to examine this aspect, the ^{238}U(n,γ) reaction cross sections from the present work and similar data from literature[14,16,18–20,26,36,50] given in EXFOR (Ref. 51) are plotted in Fig. 5. It can be seen from Fig. 5 that the ^{238}U(n,γ) reaction cross section from the present work at neutron energies of 8.04 ± 0.30 and 11.90 ± 0.35 MeV is in agreement with the value of McDaniels et al.[16] at 7.6 to 8.2 and 11.2 to 12.2 MeV, respectively.

The ^{238}U(n,γ) and ^{238}U(n,2n) reaction cross sections at different neutron energies beyond 100 keV were also calculated theoretically using the TALYS 1.4 nuclear model–based computer code.[37] TALYS can be used to calculate the reaction cross section based on physics models and parameterizations. It calculates nuclear reactions involving targets with masses >12 u and projectiles, like photons, neutrons, protons, ^{2}H, ^{3}H, ^{3}He, and alpha particles in the energy range of 1 keV to 200 MeV.

In the present work, we have used neutron energies from 100 keV to 20 MeV for the ^{238}U target using a default parameter. All possible outgoing channels for a given projectile (neutron) energy were considered including inelastic and fission channels. However, the cross sections for the (n,γ) reaction was specially looked for and collected. Theoretically calculated ^{238}U(n,γ) reaction cross sections from neutron energies of 100 keV to 20 MeV using the TALYS 1.4 version are also plotted in

Fig. 5. The theoretical $^{238}U(n,\gamma)$ reaction cross sections from TALYS are slightly higher than the experimental and evaluated values for neutron energies from 100 keV to 2 MeV. This disagreement is because in TALYS the reaction cross section as a function of neutron energy is quantitatively not well accounted, though the trend is reproduced. This may be due to the use of default parameters in the present calculation for TALYS 1.4.

In Fig. 5, the evaluated data of ENDF/B-VII.0 (Ref. 32), JENDL-4.0 (Ref. 33), JEFF-3.1/A (Ref. 34), and CENDL-3.1 (Ref. 35) are also plotted for comparison. It can be seen from the Fig. 5 that the $^{238}U(n,\gamma)$ reaction cross-section data of TALYS 1.4 produced the same trend as the evaluated data of ENDF/B-VII.0 (Ref. 32), JENDL 4.0 (Ref. 33), and JEFF-3.1/A (Ref. 34) but not of CENDL-3.1 (Ref. 35). Similarly, some of the experimental $^{238}U(n,\gamma)$ reaction cross sections are well produced by TALYS 1.4.

The experimental data of Leipunskiy et al.[18] and Panitkin and Tolstikov[19] at 1.2 to 4 MeV, Naik et al.[26] at 3.7 and 9.85 MeV, McDaniels et al.[16] at 7 to 15 MeV, and the present data at 8.04 and 11.9 MeV follow the trend of TALYS and evaluated data ENDF/B-VII.0 (Ref. 32), JENDL 4.0 (Ref. 33), and JEFF-3.1/A (Ref. 34). However, the experimental data of Leipunskiy et al.[18] and Panitkin and Tolstikov[20] at neutron energies of 5 to 7 MeV and of Panitkin and Tolstikov[20] at 17 to 20 MeV are higher than the evaluated data of ENDF/B-VII.0 (Ref. 32), JENDL 4.0 (Ref. 33), JEFF-3.1/A (Ref. 34), and theoretical values of the TALYS code.[37] Higher values at 5 to 7 MeV and 17 to 20 MeV may be due to the contribution from low-energy neutrons. This is because the experiments carried out by Leipunskiy et al.[18] and Panitkin and Tolstikov[20] are based on either D + D or D + T reactions, in which the scattered neutrons of lower energies must have contributed to the higher cross section. Something similar was observed in the present work due to lower-energy neutron tailing from the $^{7}Li(p,n)$ reaction. Thus, the contribution in the $^{238}U(n,\gamma)^{239}U$ reaction cross section due to the low-energy neutrons has been corrected in the present work, which is mentioned earlier in the calculation.

Other than the above observation, it can be seen from Fig. 5 that some of the experimental, evaluated, and theoretical $^{238}U(n,\gamma)$ reaction cross sections decrease from 100 keV to 7 MeV and predict a dip at ~7.3 to 8.5 MeV. Beyond 8.0 MeV, the cross sections increase to a neutron energy of 14 MeV and then decrease again. The dip in the $^{238}U(n,\gamma)$ reaction cross section around neutron energy of 7.5 to 8.5 MeV indicates the opening of an $(n,2n)$ reaction channel besides an (n,nf) channel. This is most probably due to the use of some part of the excitation energy in the competitive $(n,2n)$ and (n,nf) reaction channels with an (n,γ) reaction channel. To verify this, Fig. 6 plots the $^{238}U(n,2n)$ reaction cross sections from the present work and from the literature[26–29] along with the theoretical[37] and evaluated data.[32–35] It can be seen from Fig. 6 that the experimental and theoretical $^{238}U(n,2n)$ reaction cross section shows a sharp increasing trend from neutron energies of 6.16 to 8.0 MeV and thereafter remains relatively constant up to 12.0 MeV. Thus, the increasing trend of the $^{238}U(n,\gamma)$ reaction cross section beyond 8 MeV up to 14.0 MeV (Fig. 5) is due to the constant $^{238}U(n,2n)$ reaction cross section (Fig. 6). It can be also seen from Figs. 5 and 6 that the $^{238}U(n,\gamma)$ reaction cross section shows a dip, whereas the $^{238}U(n,2n)$ reaction cross section shows a sharp increasing trend. This is because in the neutron energy range below 14 MeV, the excitation energy is shared between the $^{238}U(n,\gamma)$ and $^{238}U(n,2n)$ reactions. Above the neutron energy of 14 MeV, other reaction channels such as $(n,3n)$ and $(n,2nf)$ open, and thus, both $^{238}U(n,\gamma)$ and $^{238}U(n,2n)$ reaction cross sections show a decreasing trend.

V. CONCLUSIONS

The $^{238}U(n,\gamma)^{239}U$ and $^{238}U(n,2n)^{237}U$ reaction cross sections at average neutron energies of 8.04 ± 0.30 and 11.90 ± 0.35 MeV have been determined using neutrons from the $^{7}Li(p,n)$ reaction and are in good agreement with the evaluated data from ENDF/B-VII.0, JENDL-4.0, and JEFF-3.1/A but not with CENDL-3.1.

The $^{238}U(n,\gamma)$ and $^{238}U(n,2n)$ reaction cross sections were also calculated using the TALYS 1.4 computer code and found to be in general agreement with experimentally measured data. However, in the case of the $^{238}U(n,\gamma)$ reaction, the cross-section data of TALYS 1.4 produced the same trend as the evaluated data of ENDF/B-VII.0, JENDL 4.0, and JEFF-3.1/A but not of CENDL-3.1. Similarly, the theoretical values of the $^{238}U(n,\gamma)$ reaction cross sections from TALYS 1.4 are in agreement with the experimental data at neutron energies of 1 to 4 MeV and 8 to 15 MeV but not at 4 to 7 MeV and 15 to 20 MeV.

In general, the experimental, evaluated, and theoretical cross sections for the $^{238}U(n,\gamma)^{239}U$ reaction decrease from neutron energies of 100 keV to 14 MeV with a dip at 6 to 8 MeV, whereas in the case of the $^{238}U(n,2n)^{237}U$ reaction, it sharply increases from 6.18 to 8.0 MeV, and thereafter, it remains constant up to the neutron energy of 14 MeV. Above a neutron energy of 14 MeV, other reaction channels such as $(n,3n)$ and $(n,2nf)$ open, and thus, both the $^{238}U(n,\gamma)$ and the $^{238}U(n,2n)$ reaction cross sections show a decreasing trend.

ACKNOWLEDGMENT

The authors are thankful to A. Mahadakar and D. Thapa from the target laboratory of the Pelletron facility at TIFR for providing us the Li and Ta targets. We are also grateful to the staff of the TIFR-BARC Pelletron facility for their kind

cooperation and help to provide the proton beam to carry out the experiment. One of the authors, R. Crasta, is thankful to the Board of Research in Nuclear Sciences, Department of Atomic Energy, Government of India for financial support. The authors wish to thank fellow researchers and the technical staffs at the Microtron Centre, Mangalore University for their help.

REFERENCES

1. C. RUBBIA et al., "Conceptual Design of a Fast Neutron Operated High Power Energy Amplifier," CERN/AT/95-44 (ET)1995, CERN/AT/95-53 (ET) 1995, CERN/LHC/96-01 (LET) 1996, CERN/LHC/97-01 (EET), CERN (1997).

2. S. GANESAN, "Nuclear Data Requirements for Accelerator Driven Sub-Critical Systems—A Roadmap in the Indian Context," *Pramana J. Phys.*, **68**, 257 (2007); http://dx.doi.org/10.1007/s12043-007-0029-1.

3. "Thorium Fuel Utilization: Options and Trends," IAEA-TECDOC-1319, International Atomic Energy Agency (Nov. 2002).

4. L. MATHIEU et al., "Proportion for a Very Simple Thorium Molten Salt Reactor," *Proc. 7th Int. Conf. Global 2005*, Tsukuba, Japan, October 9–13, 2005.

5. A. NUTTIN et al., "Potential of Thorium Molten Salt Reactors: Detailed Calculations and Concept Evolution with a View to Large Scale Energy Production," *Prog. Nucl. Energy*, **46**, 77 (2005); http://dx.doi.org/10.1016/j.pnucene.2004.11.001.

6. T. R. ALLEN and D. C. CRAWFORD, "Lead-Cooled Fast Reactor Systems and the Fuels and Materials Challenges," *Sci. Technol. Nucl. Install.*, **2007**, 97486 (2007); http://dx.doi.org/10.1155/2007/97486.

7. V. G. PRONYAEV, "Summary Report of the Consultants' Meeting on Assessment of Nuclear Data Needs for Thorium and Other Advanced Cycles," INDC (NDS)-408, International Atomic Energy Agency (1999).

8. B. D. KUZ'MINOV and V. N. MANOKHIN, "Status of Nuclear Data for Thorium Fuel Cycle," *Nucl. Constants*, **3–4**, 41 (1997).

9. D. E. BARTINE, "The Use of Thorium in Fast Breeder Reactors," *Proc. Int. Conf. Nuclear Cross Sections for Technology*, Knoxville, Tennessee, October 22–26, 1979, p. 119; see also NBS-SP 594, National Bureau of Standards.

10. S. PELLONI, G. YOUINOU, and P. WYDLER, "Impact of Different Nuclear Data on the Performance of Fast Spectrum Based on the Thorium-Uranium Fuel Cycle," *Proc. Int. Conf. Nuclear Data for Science and Technology*, Trieste, Italy, May 19–24, 1997, Part II, p. 1172 (1997).

11. R. BATCHELOR, W. B. GILBOY, and J. H. TOWLE, "Neutron Interactions with U^{238} and Th^{232} in the Energy Region 1.6 MeV to 7 MeV," *Nucl. Phys.*, **65**, 236 (1965); http://dx.doi.org/10.1016/0029-5582(65)90266-X.

12. H. O. MENLOVE and W. P. POENITZ, "Absolute Radiative Capture Cross Section for Fast Neutrons in ^{238}U," *Nucl. Sci. Eng.*, **33**, 24 (1968); http://dx.doi.org/10.13182/NSE68-2.

13. G. DE SAUSSURE et al., "Measurement of the Uranium-238 Capture Cross Section for Incident Neutron Energies up to 100 keV," *Nucl. Sci. Eng.*, **51**, 385 (1973); http://dx.doi.org/10.13182/NSE73-1.

14. D. DRAKE, I. BERGQVIST, and D. K. McDANIELS, "Dependence of 14 MeV Radiative Neutron Capture on Mass Number," *Phys. Lett. B*, **36**, 557 (1971); http://dx.doi.org/10.1016/0370-2693(71)90088-8.

15. R. B. PEREZ et al., "Statistical Tests for the Detection of Intermediate Structure: Application to the Structure of the ^{238}U Neutron Capture Cross Section Between 5 keV and 0.1 MeV," *Phys. Rev. C*, **20**, 528 (1979); http://dx.doi.org/10.1103/PhysRevC.20.528.

16. D. K. McDANIELS et al., "Radiative Capture of Fast Neutrons by ^{165}Ho and ^{238}U," *Nucl. Phys. A*, **384**, 88 (1982); http://dx.doi.org/10.1016/0375-9474(82)90306-2.

17. J. VOIGNIER, S. JOLY, and G. GRENIER, "Capture Cross Sections and Gamma-Ray Spectra from the Interaction of 0.5- to 3.0-MeV Neutrons with Nuclei in the Mass Range $A = 45$ to 238," *Nucl. Sci. Eng.*, **112**, 87 (1992); http://dx.doi.org/10.13182/NSE91-92N.

18. A. I. LEIPUNSKIY et al., "Measurement of Radiative Capture Cross Sections for Fast Neutrons," *Proc. 2nd Int. Conf. Peaceful Uses of Atomic Energy*, Geneva, Switzerland, September 1–13, 1958, Vol. 15, p. 50, United Nations (1958).

19. YU. G. PANITKIN and V. A. TOLSTIKOV, "Radiative Capture of Neutrons by U^{238} in the 1.2–4.0 MeV Range," *At. Energ.*, **33**, 893 (1972); http://dx.doi.org/10.1007/BF01214544.

20. YU. G. PANITKIN and V. A. TOLSTIKOV, "U^{238} Radiative Capture Cross Section for 5 to 20 MeV Neutrons,"*At. Energ.*, **33**, 945 (1972); http://dx.doi.org/10.1007/BF01666752.

21. YU. G. PANITKIN and L. E. SHERMAN, "Absolute Measurement of the Radiative Capture Cross Section of ^{238}U for 30 keV Neutrons," *At. Energ.*, **39**, 591 (1975); http://dx.doi.org/10.1007/BF01121512.

22. M. LINDNER, R. J. NAGLE, and J. H. LANDRUM, "Neutron Capture Cross Sections from 0.1 to 3 MeV by Activation Measurements," *Nucl. Sci. Eng.*, **59**, 381 (1976); http://dx.doi.org/10.13182/NSE76-2.

23. W. P. POENITZ, L. R. FAWCETT, JR., and D. L. SMITH, "Measurements of the ^{238}U(n,γ) Cross Section at Thermal and Fast Neutron Energies," *Nucl. Sci. Eng.*, **78**, 239 (1981); http://dx.doi.org/10.13182/NSE81-1.

24. N. N. BULEEVA et al., " Activation-Measured Radiative Neutron-Capture Cross Sections for ^{236}U, ^{238}U and ^{237}Np," *At. Energ.*, **65**, 920 (1988); http://dx.doi.org/10.1007/BF01121252.

25. E. QUANG and G. F. KNOLL, "Absolute Measurements of the Fast Neutron Capture Cross Section of ^{238}U," *Nucl. Sci. Eng.*, **110**, 282 (1992); http://dx.doi.org/10.13182/NSE90-99.

26. H. NAIK et al., "Measurement of the Neutron Capture Cross-Section of ^{238}U Using the Neutron Activation Technique," *J. Radoanal. Nucl. Chem.*, **293**, 469 (2012); http://dx.doi.org/10.1007/s10967-012-1815-x.

27. Y. P. CHOU, "Measurement of ^{238}U(n, 2n) Cross-Sections," Beijing Report No. 77091, China Institute of Atomic Energy (1978).

28. H. KARIUS, A. ACKERMANN, and W. SCOBEL, "The Pre-Equilibrium Contribution to the (n,2n) Reactions of ^{232}Th and ^{238}U," *J. Phys. G*, **5**, 715 (1979); http://dx.doi.org/10.1088/0305-4616/5/5/011.

29. N. V. KORNILOV et al., "Measurement of the $^{238}U(n,2n)^{237}U$ Cross Section in the Neutron Energy Range 6.5–10.5 MeV," *At. Energ.*, **49**, 722 (1980); http://dx.doi.org/10.1007/BF01120739.

30. A. A. FILATENKOV et al., "Systematic Measurement of Activation Cross Sections at Neutron Energies from 13.4 to 14.9 MeV," Report No. 252, Kholopin Radiv. Inst. Leningrad (1999).

31. X. WANG et al., "Accurate Determination of Cross Sections for $^{238}U(n,2n)^{237}U$ Induced by Neutrons Around 14 MeV," *Nucl. Instrum. Methods Phys. Res., Sect. A*, **621**, 326 (2010); http://dx.doi.org/10.1016/j.nima.2010.04.034.

32. M. B. CHADWICK et al., "ENDF/B-VII.0: Next Generation Evaluated Nuclear Data Library for Nuclear Science and Technology," *Nucl. Data Sheets*, **107**, 2931 (2006); http://dx.doi.org/10.1016/j.nds.2006.11.001.

33. K. SHIBATA et al., "JENDL-4.0: A New Library for Nuclear Science and Engineering," *J. Nucl. Sci. Technol.*, **48**, 1 (2011); http://dx.doi.org/10.1080/18811248.2011.9711675.

34. A. J. KONING et al., "The JEFF Evaluated Data Project," *Proc. Int. Conf. Nuclear Data for Science and Technology*, Nice, France, April 22–27, 2007.

35. Y. TANG et al., "China Evaluated Nuclear Data Library CENDL-3.1" (2009) (unpublished); see also Z. G. GE et al., "The Updated Version of Chinese Evaluated Nuclear Data Library (CENDL-3.1)," *Proc. Int. Conf. Nuclear Data for Science and Technology*, Jeju Island, Korea, April 26–30, 2010.

36. D.-Z. DING and T.-C. GUO, "Review of ^{238}U Capture Cross-Sections En=1 keV to 20 MeV," Beijing Report No.77106, Institute of Atomic Energy (1978).

37. A. J. KONING, S. HILAIRE, and M. C. DUIJVESTIJN, "TALYS: Comprehensive Nuclear Reaction Modeling," *AIP Conf. Proc.*, **769**, 1154 (2005); http://dx.doi.org/10.1063/1.1945212.

38. H. LISKIEN and A. PAULSEN, "Neutron Production Cross Sections and Energies for the Reactions $^{7}Li(p,n)^{7}Be$ and $^{7}Li(p,n)^{7}Be^{*}$," *At. Data Nucl. Data Tables*, **15**, 57 (1975); http://dx.doi.org/10.1016/0092-640X(75)90004-2.

39. J. W. MEADOWS and D. L. SMITH, "Neutrons from Proton Bombardment of Natural Lithium," ANL-7983 919720, Argonne National Laboratory.

40. C. H. POPPE et al., "Cross Section for the $^{7}Li(p, n)^{7}Be$ Reaction Between 4.2 and 26 MeV," *Phys. Rev. C*, **14**, 438 (1976); http://dx.doi.org/10.1103/PhysRevC.14.438.

41. S. G. MASHNIK et al., "$^{7}Li(p, n)$ Nuclear Data Library for Incident Proton Energies to 150 MeV," Los Alamos National Laboratory (Feb. 8, 2008).

42. "International Reactor Dosimetry File: IRDF-2002," Nuclear Data Section, International Atomic Energy Agency (2002).

43. S. NAGY et al., "Mass Distributions in Mono-Energetic Neutron-Induced Fission of 238U," *Phys. Rev. C*, **17**, 163 (1978); http://dx.doi.org/10.1103/PhysRevC.17.163.

44. M. RAJAGOPALAN et al., "Mass Yields in the 14 MeV Neutron-Induced Fission of ^{238}U," *J. Inorg. Nucl. Chem*, **38**, 351 (1976); http://dx.doi.org/10.1016/0022-1902(76)80434-4.

45. W. D. ALLEN and A. T. G. FERGUSON, "The Fission Cross Sections of ^{233}U, ^{235}U, ^{238}U and ^{239}Pu for Neutrons in the Energy Range 0.030 MeV to 3.0 MeV," *Proc. Phys. Soc. A*, **70**, 573 (1957); http://dx.doi.org/10.1088/0370-1298/70/8/303.

46. R. B. FIRESTONE and L. P. EKSTROM, *Table of Radioactive Isotopes* (2004); see also E. BROWNE and R. B. FIRESTONE, *Table of Radioactive Isotopes*, V. S. SHIRLEY, Ed., John Wiley and Sons, New York (1986).

47. M. R. SCHMORAK, "Nuclear Data Sheets for A = 231, 235, 239," *Nucl. Data Sheets*, **40**, 1 (1983); http://dx.doi.org/10.1016/S0090-3752(83)80080-5.

48. Y. A. AKOVALI, "Nuclear Data Sheets for A = 237," *Nucl. Data Sheets*, **74,** 461 (1995); http://dx.doi.org/10.1006/ndsh.1995.1014.

49. P. K. MUKHOPADHYAYA, Personal Communication (2001).

50. V. H. TAN, N. C. HAI, and N. T. HIEP, "Measurement of Capture Cross Sections of ^{238}U on the Filtered keV-Neutron Beams," Report No. 8, International Nuclear Data Committee (1996).

51. IAEA-EXFOR Database: http://www-nds.iaea.org/exfor.